

# **Impact of Cloud Analysis on Numerical Weather Prediction in the Galician Region of Spain**

M. J. SOUTO, C. F. BALSEIRO AND V. P. REZ-MU—UZURI

*Group of Nonlinear Physics, Faculty of Physics, University of Santiago de Compostela,  
Santiago de Compostela, Spain*

Ming Xue

*University of Oklahoma, School of Meteorology, and CAPS  
Oklahoma, USA*

Keith BREWSTER

*Center for Analysis and Prediction of Storms, Oklahoma, USA*

April, 2001

Revised December, 2001

*Corresponding author address:* Dra. M. J. Souto, Group of Nonlinear Physics  
Faculty of Physics, University of Santiago de Compostela  
E-15706, Santiago de Compostela, Spain  
e-mail: [uscfamsa@cesga.es](mailto:uscfamsa@cesga.es)

## **ABSTRACT**

The Advanced Regional Prediction System (ARPS) is applied to operational numerical weather forecast in Galicia, northwest Spain. A 72-hour forecast at a 10-km horizontal resolution is produced dta for the region. Located on the northwest coast of Spain and influenced by the Atlantic weather systems, Galicia has a high percentage (almost 50%) of rainy days per year. For these reasons, the precipitation processes and the initialization of moisture and cloud fields are very important. Even though the ARPS model has a sophisticated data analysis system (ADAS) that includes a 3D cloud analysis package, due to operational constraint, our current forecast starts from 12-hour forecast of the NCEP AVN model. Still, procedures from the ADAS cloud analysis are being used to construct the cloud fields based on AVN data, and then applied to initialize the microphysical variables in ARPS. Comparisons of the ARPS predictions with local observations show that ARPS can predict quite well both the daily total precipitation and its spatial distribution. ARPS also shows skill in predicting heavy rains and high winds, as observed during November 2000, and especially in the prediction of the November 5th, 2000 storm that caused widespread wind and rain damage in Galicia.

## 1. Introduction

Located on the northwest of Spain and influenced by the Atlantic weather systems, Galicia has a high percentage (almost 50%) of rainy days per year. The monthly mean number of days with precipitation of 1 mm or more, and the annual average (last column) measured at five different sites marked as A, B, C, D, E in Fig. 1c for the period 1961-1990 are shown in Table 1. One can see that between October and May nearly all locations have rain in more than 50 percent of the days.

Galicia is located in a region of complex terrain and a wide variation in land use. Two typical synoptic situations exist in the region (Mounier, 1964, 1979). In the summer, the region is primarily affected by the Azores high pressure center, with associated northwestern winds and clear sky. In the winter, it is mainly affected by cold fronts associated with the typical low pressure center located over Britain. Ahead of the front southwesterly winds are found. Convective precipitation is not very typical in the region, with heavy convective precipitation occurring only a few days per year. In the winter season, the precipitation in this area is influenced largely by the passage of cold fronts from the Atlantic Ocean and the interaction of these systems with local topography. The fronts are usually associated with extratropical cyclones whose centers are generally located further north. The topography of this region is shown in Figure 1, where one can see the wide variation in terrain on small scales. For example, there is a mountain chain located in the southeast, only 200 km from the coast, with peaks of more than 1600 meters. There are also altitudes of about 500 meters located in the northern part of the region just 20 km from the coast. The coastal bays, called rias, that characterize the southwest coastline also have a strong influence on the local weather.

For these reasons, detailed forecasts of precipitation are very desirable for this region, and we seek to investigate the forecasting of rainfall using a high-resolution nonhydrostatic numerical model and study the impact of the moisture and cloud initialization. Several studies have suggested that mesoscale models run at high resolutions can realistically predict precipitation over complex terrain (Bruitjes et al. 1994; Colle and Mass 1996; Gaudet and Cotton 1998; Colle et al. 1999; Buzzi et al 1998; Sandvik 1998).

Initialization of cloud water content in a high-resolution numerical model is a significant issue and so far, most numerical weather prediction (NWP) models do not initialize it using observations. The simplest procedure for initializing cloud water is to start with zero values at all grid points and let the model gradually build up cloud mass. Thus, the model must 'spin-up' or create cloud water/ice during the first few hours. This creates a lag in the development of precipitation as the air must reach saturation or near saturation in the presence of cumulus parameterization scheme before precipitation can occur. Models that do include the cloud water as a prognostic variable may carry the field (from forecast background) in the data analysis process into the next prediction cycle. Without the use of additional information, such forecast fields may be in error, however. One previous related study (Kristjansson, 1992) concluded that the initialization of the cloud water field by itself does not have a large effect on the spin-up of precipitation and clouds, and a much larger effect is obtained when the humidity field is enhanced. In Colle et al., 1999, when the MM5 model was initialized with a cold start (i. e., no hydrometeors and significant ageostrophic motions), it took 12-18 h on average for the model

precipitation to spin up. To avoid the spinup issue, Colle et al (2000) compared forecasts in the 8-44 hour range when they studied the effect of grid spacing, vertical resolution and five different microphysical schemes.

In recent years, most operational NWP centers have developed or are developing advanced data assimilation systems based on optimal interpolation, 3D-Var and 4D-Var techniques, with limited success in assimilating cloud and precipitation data. For example, only radiosonde humidity data are used operationally at present by HIRLAM model, and are assimilated by optimal interpolation (OI, Amstrup and Huang, 1999). At Meteo-France, the operational Aladin and Arpege models currently use a 3D-Var system and use only radiosondes and HIRS-11/12 humidity information in their upper air assimilation (Courtier *et al.*, 1991). The ETA model of NCEP, NOAA has been using 3D-Var since Feb.1998. The model has prognostic cloud water and it is passed on from previous analysis times through the EDAS (Eta Data Assimilation System) cycle. It uses radiosonde, surface reports, DMSP (Defense Meteorological Satellite Program ) SSM/I TCWV and GOES TCWV (Total Column Water Vapor) in the analysis. The system performs direct assimilation of GOES and polar satellite radiances in the 3D-Var and uses observed hourly precipitation and cloud top pressure in its 3-hourly cycle. At NCAR, a recent investigation explores the impact of the assimilation of satellite-retrieved soundings on forecast error in the MM5 model: combinations of conventional surface and radiosonde observations and retrieved temperature and moisture soundings from the DMSP and Television and Infrared Observation Satellite Operational Vertical Sounder (TOVS) satellite instruments are assimilated employing the four-dimensional data assimilation technique. (Powers and Gao, 2000). At NCEP, satellite-retrieved rainfall is assimilated into its Medium Range Forecast (WRF) model (Falkovich *et al.*, 2000) using the NCEP GDAS (Zapotocnt et al 2000). Observations are inserted into the system every 6 hours. At ECMWF, 4D-Var was implemented in November 1997. Work has been done on the problem of cloud analysis in the context of advanced variational data assimilation. For example, in Janiskova (2001), 1D-Var experiments using simulated observations were performed to investigate the potential of radiation and cloud schemes to modified model temperature, humidity and cloud profiles in order to better match observations of radiation fluxes. Feasibility studies in a 1D-Var framework using data from field experiments that measures of both cloud properties and radiative fluxes have also been carried out.

At the Center for Analysis and Prediction of Storms (CAPS), University of Oklahoma, in order to provide detailed initial conditions for moisture variables in the ARPS (Advanced Regional Prediction System), (Xue *et al.*, 1995, 2001), and to serve as the basis for moisture data assimilation, a cloud analysis procedure has been developed within the ARPS Data Analysis System (ADAS, Brewster, 1996). The cloud initialization procedure is a customization of the algorithms used by the Forecast Systems Lab in the Local Analysis and Prediction System (LAPS, Albers, 1996) with certain enhancements and refinements (Zhang *et al.*, 1998, 1999). It incorporates cloud reports from surface stations reporting World Meteorological Organization (WMO) standard Aviation Routine Weather Reports (METARs), satellite infrared and visible imagery data, and radar reflectivity to construct three-dimensional cloud and precipitation fields. The products of the analysis package include three-dimensional cloud cover, cloud liquid and ice water mixing ratios, cloud and precipitate types, in-cloud vertical velocity, icing severity index, and rain/snow/hail mixing ratios. Cloud base, top and cloud ceiling fields are also derived.

In this work, ARPS application to an operational numerical weather forecast in Galicia (Spain) is described. Even though the ARPS model has ADAS, a sophisticated data analysis system that includes a three-dimensional cloud analysis package, due to operational constraints, our current forecast starts from the 12-hour forecast of NCEP AVN model. Still, procedures from the ADAS cloud analysis are being used to construct the cloud fields based on AVN forecast data, and a three-category ice microphysics scheme is used in the ARPS operational runs. The next section describes the operational implementation, and the governing equations are presented on Section 3. The cloud analysis procedure is explained on Section 4, while Section 5 and 6 present and summarize the results.

## 2. Operational Implementation

The ARPS is applied to an operational numerical weather forecast in Galicia (Spain). The ARPS model was chosen because its nonhydrostatic dynamics, generalized terrain following coordinate, and its nesting capabilities are well suited for the complexities of the Galician region. ARPS had also been tested quasi-operationally for several years, especially for convective seasons, at CAPS (Droegemeier *et al.*, 1996; Xue *et al.*, 1996; Carpenter *et al.*, 1999). For this application, the nesting was set up to permit the resolution of flows at two scales: the influence of local terrain features in the 10-km fine grid, and the mesoscale circulations (particularly those concerning the passage of cold fronts from the Atlantic Ocean) by the 50-km coarse grid. The general scheme of the daily 72-hour forecast is schematically depicted in Fig. 2. The ARPS model starts from enhanced 12-hour forecast of NCEP AVN model, and uses the boundary conditions also obtained from NCEP AVN model at three hours interval on a coarse grid covering a  $1500 \times 1500 \text{ km}^2$  area (Fig. 1b). Within this coarse domain is nested the fine grid covering a  $400 \times 400 \text{ km}^2$  area (Fig. 1c). In the vertical, there are 43 sigma-z levels extending to 21km. The fine grid uses its own higher-resolution terrain with transitions to the coarse grid terrain in a boundary zone for better match of solutions. The initial condition of the coarse grid is interpolated to fine-grid grid points using linear and quadratic interpolation for vertical and horizontal respectively. The 12-hour AVN forecast instead of analysis is used due to operational time constraints. We do not receive the AVN data set until ??? hours after the analysis time. It was not possible for us to use the AVN analysis and still be able run the nested models and produce forecasts for the same day. The forecast had to be available at the first hour in the morning. We plan in the future to run the model twice daily, using the 00-hour and 12-hour AVN output. Forecasts on the two grids take approximately 8 hours of CPU time on a Fujitsu VPP300E computer using the sole processor available to the project. Adding the time needed for plotting and web posting, the process takes a total of 10 hour wallclock time. The forecasts for the present day, the next day, and the subsequent day are ready for the weather forecasters and general public on the Galician regional forecast web site (<http://meteo.usc.es>) at about 0500UTC daily (i.e., 6 am local time).

## 3. The Governing Equations

The governing equations of the ARPS include conservation equations for momentum, heat, mass, water substance (water vapor, liquid and ice), subgrid scale (SGS) turbulent kinetic energy (TKE), and the equation of state of moist air. The modified three-category ice scheme of Lin *et al.* (1983) is used for microphysics parameterization. It includes two liquid phases (cloud and rain) and three ice categories (ice cloud, snow and

hail or graupel). The implementation of the Lin scheme follows that of Tao and Simpson (1993) and includes the ice-water saturation adjustment procedure of Tao *et al.* (1989). The source terms corresponding to the conservation equation of water substances  $q_c$  (cloud water),  $q_r$  (rain),  $q_i$  (cloud ice),  $q_s$  (snow) and  $q_h$  (hail/graupel) include the following conversion terms based on:

$$S_{q_c} = \rho(c - e_c) - T_{q_c} \quad (1)$$

$$S_{q_r} = \rho(-e_r + m_s + m_h - f_s - f_h) - T_{q_r} \quad (2)$$

$$S_{q_i} = \rho(d_i - s_i) - T_{q_i} \quad (3)$$

$$S_{q_s} = \rho(d_s - s_s - m_s + f_s) - T_{q_s} \quad (4)$$

$$S_{q_h} = \rho(d_h - s_h - m_h + f_h) - T_{q_h} \quad (5)$$

The symbols  $c$ ,  $e$ ,  $f$ ,  $m$ ,  $d$  and  $s$  denote the rates of condensation, evaporation of droplets, freezing of raindrops, melting of snow and graupel, deposition of ice particles, and sublimation of ice particles, respectively. Specific species are identified by the subscripts, with  $c$ ,  $r$ ,  $i$ ,  $s$  and  $h$  representing cloud, rain, ice, snow and hail, respectively. The terms  $T_{q_c}$ ,  $T_{q_r}$ ,  $T_{q_i}$ ,  $T_{q_s}$  and  $T_{q_h}$  are microphysical transfer rates between the hydrometeor species and their sum is zero. The complicated transfers encompass nearly thirty processes. They include autoconversion, which parameterizes the collision-coalescence and collision-aggregation, and accretion among the various forms of liquid and solid hydrometeors. The transformation of cloud ice to snow through autoconversion (aggregation), the Bergeron processes (Bergeron, 1935), and subsequent accretional growth or aggregation to form hail are simulated. Hail is also produced by various contact mechanisms and via probabilistic freezing of raindrops. Evaporation (sublimation) is considered for all precipitation particles outside the cloud. The melting of hail and snow, wet and dry growth of hail and shedding of rain from hail are included. The complete formulation of each of the transfers can be found in Lin *et al.* (1983). More details on the model formulation can be found in Xue *et al.* (1995) and Xue *et al.* (2000).

#### 4. Cloud Analysis Procedure

For our purposes, a three-dimensional background cloud cover field on the 50-km coarse grid is derived from the relative humidity values in the initial and boundary condition fields using an empirical power relationship similar to one used in Koch *et al.* (1997):

$$CF = \left( \frac{RH - RH0}{1.0 - RH0} \right)^b \quad (6)$$

Here  $CF$  is the cloud fractional cover that ranges from 0.0 to 1.0,  $RH$  is the relative humidity,  $RH0$  is a relative humidity threshold whose value is dependent on the height and  $b$  is an empirical constant. In this case,  $b$  is set to 2. The relationships between cloud cover and  $RH$  as a function of height,  $z$ , used in this work are depicted in Fig. 3.

After the three-dimensional cloud cover distribution is obtained, values for the various cloud species are calculated using the same procedures employed in the ADAS cloud scheme for regions where directly observed cloud information is lacking. The procedure follows modified LAPS cloud scheme (Albers *et al.*, 1996) as is given in Zhang *et al.* (1998; 1999). For each grid column, cloud tops and bases are determined for layers having a cloud coverage that exceeds a threshold value (0.5 in this case). The adiabatic

liquid water content (ALWC) is the maximum value of liquid water content in the cloud based solely on thermodynamic processes, taking into account the change in liquid water due to the change in the saturation mixing ratio. ALWC is estimated by assuming moist adiabatic conditions throughout the cloud and is calculated for each grid point (and accumulated) from the base upward. This adiabatic computation of LWC consists of several steps. From cloud base the moist adiabatic lapse rate is used to calculate the temperature in 50m increments above cloud base. These temperatures define the saturation vapor pressures at 50m increments through the cloud. The difference in saturation vapor pressure over a 50m interval defines the additional condensed moisture that is accumulated beginning at cloud base and continuing to the cloud top. Then an entrainment reduction curve (Fig. 4) is applied which reduce the ALWC by 40% near the cloud base and by 75% at about 500 m above the cloud base. Constant 80% reduction is applied for levels 1.5 km or more above the cloud base. The reduced ALWC is defined as cloud liquid water when temperature is warmer than  $\bar{n}10^{\circ}\text{C}$ , and as cloud ice when temperature is colder than  $\bar{n}30^{\circ}\text{C}$ . A linear ramp is applied for the temperature in between. The specific humidity at those grid points that contain cloud water is saturated, so that the conditions for cloud formation in the condensation scheme of the model are satisfied.

Finally, a latent heat adjustment to temperature based on added ALWC ( $\Delta T$ ) is applied, according to the formula

$$\left. \begin{aligned} \Delta T_{q_c} &= a \cdot \Delta q_c, & a &= f_{q_c} \cdot L_v / C_p \\ \Delta T_{q_i} &= b \cdot \Delta q_i, & b &= f_{q_i} \cdot (L_v + L_f) / C_p \end{aligned} \right\} \Delta T = \Delta T_{q_c} + \Delta T_{q_i} \quad (7)$$

where  $f_{q_c}$  and  $f_{q_i}$  are constants for adjusting the fraction of latent heat added from  $q_c$  and  $q_i$  respectively, (in this case equal to 0.8),  $L_v$  and  $L_f$  are the latent heat of vaporization and fusion at  $0^{\circ}\text{C}$ , respectively, and  $C_p$  is the specific heat of dry air at constant pressure.

## 5. A Representative Case

The period from November 2000 to mid-February 2001 was characterized by very inclement weather over Galicia. Active cold fronts coming from the Atlantic Ocean caused very strong southwesterly winds with heavy rains over the entire region, especially in the southwest due to orography. During this period, Galicia experienced 20 days of severe weather, including warnings for severe rain and wind. A wind warning is issued when the mean wind velocity in the coastal areas is higher than 80 km/h ( $22 \text{ ms}^{-1}$ ) and a rain warning when precipitation greater than 30 mm is accumulated in one hour or 60 mm in twelve hours. Galicia is not a very large region, but it has a very complex topography that determines the spatial distribution of precipitation. This fact complicates the precipitation forecast. In Fig. 5, one can see large differences among total accumulated precipitation measurements (numbers in the boxes) for November 2000 depending on the location. High values of precipitation, exceeding 900 mm, accumulated in the southwest where moist air from the sea runs over with the mountains. By contrast, just over 100 mm accumulated in northeast part of Galicia in a region of terrain rain shadowing. We will come back to this figure later.

In this work, we present the results obtained with ARPS model and demonstrate the importance of the cloud initialization for the Galician operational forecast in a period of severe weather -- not only in the daily total precipitation but also in its spatial distribution. For brevity, we present here the results for November 2000, and particularly,

the storm that occurred on 5 November 2000. The synoptic situation for that day is shown in Fig. 6, which is taken from the INM (National Weather Service of Spain) bulletins. A cold front associated with a deep low centered on the southwest of the British Islands passed through Galicia, causing strong southwesterly winds and heavy rains over the entire region. This situation can be considered representative of the general synoptic pattern during entire November 2000. This synoptic pattern was well described by ARPS, as it is shown in Fig. 7, where sea level pressure (contours) and 850hPa temperature (shaded field) predicted by ARPS (0-24 h forecast) on 50 km coarse grid for 5 November, 2000 at 0600UTC, 1200UTC and 1800UTC are shown: ARPS model predicted quite well the location of both cold and warm fronts as compared to the analysis in Fig. 6.

As shown in Fig. 6, at 1200UTC the cold front is just arriving in northwest Galicia, a cold front with a band of cumulonimbus convection along it. This situation was well predicted by ARPS. As is shown in Fig. 8a, ARPS predicted a band of high vertically integrated rain water mixing ratio ( $q_r$ ) at the observed frontal location, in the run where the cloud generation at the initial and boundary conditions is included. Without the cloud initialization, the model was not able to predict the frontal precipitation, so the  $q_r$  values obtained at the same time are smaller throughout domain, specially in the northwestern corner, near the front. (Fig. 8b).

In Fig. 9 the surface wind field forecasted by the ARPS model for 1500UTC 5 November 2000 is shown. The model produced strong southwesterly winds, with values around  $20 \text{ ms}^{-1}$  in the northern coastal areas (wind gusts higher than  $30 \text{ ms}^{-1}$  were measured in coastal towns). A comparison between observed and forecasted wind velocity and direction for 5 November 2000 is shown for two locations marked A (on the west coast, 5m elevation) and B (in the southeast mountains, 970 m elevation) is shown in Fig. 10. The ARPS model predicted the observed increase in wind velocity in the afternoon and maintained the southwesterly winds during all the day at both locations.

## 6. Verification

The Galician meteorological network, consisting of 43 climatological stations and 22 meteorological surface stations covering the entire region, was used to verify the model forecasts. In Fig. 5, the total rainfall predicted with ARPS model for the month of November is contoured and is compared with observations (numbers in boxes). ARPS forecasts using cloud initialization agree quite well with predictions not only in quantitative amount but also the geographical distribution. ARPS predicted very high values of precipitation in the southwest area of the region, where moist air from the sea is brought in by the southwest winds (see Fig. 9) to be lifted over the topography and produced values of precipitation greater than 800 mm, very close to the measurement maximum of 922 mm. In the mountainous areas of the southeast, the model also predicted the high values of precipitation measured, around 600 mm, and correctly distinguished the valley zones with values of only 200 mm. In the north part of the region, the model also produced a good forecast and reproduced the significant precipitation (593 mm) that occurred in the mountainous area located in the center, and the drier zones on each side of this mountain. The minimum value of 110 mm measured at the northeast matches very well the forecast of 100 mm from ARPS. On the other side, in the northwest, ARPS predicted precipitation of around 250 mm that also agreed quite well with the measured values.

Focusing on a particular day, we can see more clearly the importance of the cloud initialization in the precipitation forecast. In Figs 11(a) and 11(b) the total precipitation rainfall predicted with and without cloud initialization, respectively, is compared with measurements (numbers in boxes) for 5 November 2000. At first glance, there is an important difference in the values obtained over the sea: with the cloud initialization (a) a more realistic distribution is obtained, because it shows significant rainfall values in the west, where the cold front is; but, without it (b) the model does not represent correctly the frontal clouds, and it generates less rainfall. Although the rainfall spatial distribution over the terrain is similar in both cases, the quantitative forecast is better in case (a), as we can see, for example, in the mountainous area located in the north, where 118 mm were measured and the predicted value was near 110 mm, while in case (b) the predicted value was about 80 mm. Also, in the mountainous area located in the southeast, 116 mm and 78 mm were measured at neighboring points and ARPS predicted values in case (a) around 110 mm and 80 mm respectively, while, in case (b) the model-predicted precipitation was less than 80 mm. This accurate forecast of the rainfall maxima is very important for alerting the public about the threat of heavy rainfall.

The effect of cloud water initialization is also demonstrated in Fig. 12, which shows the enhancement of the 500 hPa equivalent potential temperature and analyzed frontal positions for 5 November 2000, 1500 UTC. The enhancement is greatest in the frontal zone in the eastern part of the region, where the differences reach values of about 2K.

The daily total precipitation predicted by ARPS for November, 2000 is compared with measurements at three representative surface stations in Fig. 13. We consider them representative because they are located at very different locations in the region and at different heights above sea level: MOUR (Mouriscade, Pontevedra, 490m), INVE (Invernadeiro, Ourense, 1020m) and PMUR (Pedro Murias, Lugo, 43 m) (M, I, P in Fig.1, respectively). In all cases, the model was able to follow the daily evolution of the precipitation and to accurately distinguish with accuracy the heavy and light rainy days. It is interesting to note the important differences between INVE station, located in a southeast mountainous of Galicia, with only one day of no-precipitation and a daily mean value of about 25 mm, and PMUR station, located on the coast, in the northeast portion of the region, with eight days of no-precipitation and a daily mean value of only 4 mm. The model appears to have good skill in reproducing these differences. It is also shown in Fig. 14 the precipitation time series (predicted and measured) at MOUR location for 5<sup>th</sup> November 2000: with the cloud initialization applied at the initial conditions and cloud water enhancement in the (WRF forecast) boundary conditions, the predicted values agree quite well with measurements during the entire 24 hour time period.

In Fig. 15, the scattergram plots of observed precipitation (mm) and forecasts for 5th November 2000 with and without cloud initialization summarize the model precipitation performance: light precipitation is well predicted in both cases but the cloud initialization improved the heavy precipitation forecast significant. For values bigger than 60 mm, the precipitation in the latter case is significantly under-predicted while the case with cloud initialization produced a much better fit between the forecast and observation. In general, the case without cloud initialization has a significant low bias in precipitation amount while that case with cloud initialization tends to slightly over-predict the precipitation but the absolute bias is much smaller.

We further formally verify precipitation forecast using bias and threat scores. The bias score  $B = F/O$  is the ratio of the number of stations forecasted to reach or exceed a certain precipitation threshold ( $F$ ) to the number of stations that actually exceed the threshold ( $O$ ); a perfect forecast would have  $B=1$ , while values of  $B$  less than and greater than one represent underforecasting and overforecasting, respectively, the precipitation areal coverage. A limitation of the bias score is that it does not provide a measure of the coincidence of stations for which precipitation was forecasted with those at which it is observed; this can be measure through a threat score,  $T$ , defined as:

$$T = \frac{CF}{F + O - CF} \quad (8)$$

where  $CF$  is the number of correctly forecast stations (both model and observations produce precipitation at or above a given threshold), and  $F$  and  $O$  are as defined above. (Gaudet and Cotton, 1998). Table 2 contains these skill scores for November, 2000. At low precipitation thresholds, both  $B$  and  $T$  values are close to one, and are exactly one for November 5, when an important storm occurred. For this day, the model slightly overestimated the areal coverage of heavy rain (e. g.,  $B=1.75$  for 50 mm threshold) and predicted quite well the geographical location ( $T=0.57$  for 50 mm threshold). Note that for all thresholds, the same ten stations are being considered.

The monthly mean value of bias and threat score for various precipitation thresholds (mm/24h) for November, 2000 are shown in Fig. 16. For low thresholds, the results imply good skill for rain/no-rain forecast and its location, while for larger thresholds, the model loses some precision in the geographical location of the precipitation, but maintains good bias scores.

## 7. Summary and Conclusions

The Advanced Regional Prediction System (ARPS) has been applied to operational numerical weather forecast in Galicia, in Northwestern Spain since January, 2000. Due to the high percentage of rainy days per year in this region, the precipitation processes and the initialization of clouds and moisture in the model is very important. A cloud analysis procedure developed in the ARPS Data Analysis System (ADAS) was used to construct the cloud fields based on forecast relative humidity from the global AVN model of NCEP. The cloud fields were used to initialize the microphysical variables in the ARPS. A three-category ice scheme that includes two liquid phases (cloud and rain) and three ice categories (ice cloud, snow and hail or graupel) is used for microphysics parameterization in ARPS.

Comparisons of the ARPS predictions with local observations show that both the daily total precipitation and its spatial distribution were predicted reasonably well. The latter is very challenging at this region, as it is shown by the large spatial variations in the observed precipitation rates. ARPS also shows skill in predicting heavy rains and high winds, as were observed during most of November 2000, and exemplified by the prediction of the 5 November, 2000 storm in Galicia. In this specific case, as well as in the monthly values, The model successfully reproduced the influence of the complex local terrain features and the mesoscale circulations that combine to produce the complex spatial distribution of the rain in Galicia for this specific case as well as in the monthly values. It was also shown for this case that the both the precipitation pattern and amount were improved when cloud analysis procedure is employed. We do caution here that it takes a comparison of long term statistics of parallel forecasts, one with and one without

cloud analysis, to arrive at more convincing conclusions. Unfortunately, a strict limitation of computational resources precludes this option for us, at least in the near future. Our experience does suggest that quantitative precipitation forecast was improved after the cloud analysis procedure was introduced into the forecast system.

### ***Acknowledgments***

This work is supported by the Department of Environment of the Galician Government (Xunta de Galicia) as part of its Observational and Meteorological Forecasting Unit.

### ***References:***

- Albers, S. C., J. A. McGinley, D. A. Birkenheuer, and J. R. Smart, 1996: The local analysis and prediction system (LAPS): Analysis of clouds, precipitation and temperature. *Wea. Forecasting*, **11**, 273-287
- Amstrup, B. and Xiang-Yu Huang, 1999: Impact of the additional FASTEX radiosonde observations on the High-Resolution Limited-Area Model (HIRLAM) data-assimilation and forecasting system. *Quart. J. Roy. Meteor. Soc.*, **125**, 3359-3374
- Bergeron, T., 1935: On the physics of cloud and precipitation. *Proc. 5th Assembly of IUGG*, Lisbon, 156-178
- Brewster, K., 1996: Implementation of a Bratseth analysis scheme including Doppler radar. *Preprints, 15<sup>th</sup> Conf. On Weather Analysis and Forecasting*, AMS, Boston, 92-95.
- Bruintjes, R. T., Clark, T. L. and May W. D., 1994: Interactions between topographic airflow and cloud/precipitation development during the passage of a winter storm in Arizona. *J. Atmos. Sci.*, **51**, 48-67
- Buzzi, A., Tartaglione, N. and Malguzzi, P., 1998: Numerical simulations of the 1994 Piedmont flood: role of orography and moist processes. *Mon. Wea. Rev.*, **126**, 2369-2383.
- Carpenter, R. L. J., Droegemeier, K. K., Basset, G. M., Weygandt, S. S., Jahn, D. E., Stevenson, S., Qualley, W. and Strasser, R., 1999: Storm-scale numerical weather prediction for commercial and military aviation, Part I: Results from operational tests in 1998. *Preprints, 8<sup>th</sup> Conf. on Aviation, Range, and Aerospace Meteorology*. Amer. Meteor. Soc., Dallas, TX, 209-211.
- Colle, B. A. and Mass, C. F., 1996: An observational and modeling study of the interaction of low-level southwesterly flow with the Olympic Mountains during COAST IOP 4. *Mon. Wea. Rev.*, **124**, 2152-2175
- Colle, B. A., Weatrick, K. J. and Mass, C. F., 1999: Evaluation of MM5 and Eta-10 precipitation forecast over the Pacific Northwest during the cool season. *Wea. Forecasting*, **14**, 137-154
- Colle, B. A. and Mass, C. F., 2000: The 5-9 February 1996 flooding event over the Pacific Northwest: sensitivity studies and evaluation of the MM5 precipitation forecast. *Mon. Wea. Rev.*, **128**, 593-617
- Courtier, P., Freyrier, C., Geleyn, J-F., Rabier, F. and Rochas, M., 1991: The Arpege project at Météo-France, *Proc. ECMWF Workshop on numerical methods in atmospheric model, Reading, 9-13 September, 193-231, Available from ECMWF, Shinfield, Reading, UK.*

- Droegemeier, K. K., Xue, M., Brewster, K., Liu, Y., Park, S., Carr, F., Mewes, J., Zong, J., Sathye, A., Bassett, G., Zou, M., Carpenter, R., McCarthy, D., Andra, D., Janish, P., Graham, R., Sanielvici, S., Brown, J., Loftis, B. and McLain, K., 1996: The 1996 CAPS spring operational forecasting period: Realtime storm-scale NWP, Part I: Goals and methodology. *Preprint, 11<sup>th</sup> Conf. on Num. Wea. Pred.* Amer. Meteor. Soc., Norfolk, VA, 294-296
- Falkovich, A., Kalnay, E., Lord S. and Mathur, M. B., 2000: A new method of observed rainfall assimilation in forecast models. *J. Appl. Meteor.*, **39**, 1282-1298
- Gauden, B. and Cotton, W. R. 1998. Statistical characteristics of a real-time precipitation forecasting model. *Wea. Forecasting*, **13**, 966-982.
- Janiskova, M., 2001: Preparatory studies for the use of observations from the Earth radiation Mission in NWP. *ESA Contract report No. 13151/98/NL/GD, available from ECMWF.*
- Koch, S. E., A. Aksakal, and J. T. Mcqueen, 1997: The influence of mesoscale humidity and evapotranspiration fields on a model forecast of a cold-frontal squall line, *Mon. Wea. Rev.*, **125**, 384-409
- Kristjansson, J. E., 1992: Initialization of cloud water in a numerical weather prediction model. *Meteor. Atmos. Phys.*, **50**, 21-30
- Lin, Y.-L., R. D. Farley, and H. D. Orville, 1983: Bulk parameterization of the snow field in a cloud model. *J. Climate Appl. Meteor.*, **22**, 1065-1092
- Mounier, J., 1964: La saison pluviométrique indigène dans les régions océaniques du Sud-Ouest de l'Europe, Bretagne et Galice. *Norois*, Jul-Sep.:261-282
- Mounier, J., 1979: La diversité des climats océaniques de la Péninsule Iberique. *La Meteorologie*, Serie 6, **106**: 205-227
- Powers, J. G. and Gao, K., 2000: Assimilation of DMSP and TOVS satellite soundings in a mesoscale model. *J. Appl. Meteor.*, **39**, 1727-1741
- Sandvik, A. D., 1998: Implementation and validation of a condensation scheme in a nonhydrostatic mesoscale model. *Mon. Wea. Rev.*, **126**, 1882-1905
- Tao, W.-K., J. Simpson, and M. McNumber, 1989: An ice-water saturation adjustment. *Mon. Wea. Rev.*, **117**, 231-235
- Tao, W.-K. And J. Simpson, 1993: Goddard cumulus ensemble model. Part I: Model description. *Terr. Atmos. Ocean Sci.*, **4**, 35-72
- Xue, M., K. K. Droegemeier, V. Wong, A. Shapiro, K. Brewster, 1995: ARPS Version 4.0 User's Guide.
- Xue, M., Brewster, K., Droegemeier, K. K., Wong, V., Wang, D. H., Carr, F., Shapiro, A., Zhao, L. M., Weygandt, S., Andra, D. and Janish, P., 1996: The 1996 CAPS spring operational forecasting period: Realtime storm-scale NWP, Part II: Operational summary and examples. *Preprint, 11<sup>th</sup> Conf. on Num. Wea. Pred.* Amer. Meteor. Soc., Norfolk, VA, 297-300

- Xue, M., K. K. Droegemeier and V. Wong, 2001: The Advanced Regional Prediction System (ARPS)- A multiscale nonhydrostatic atmospheric simulation and prediction tool. Part I: Model dynamics and verification. *Meteor. Atmos. Phys.*, **75**, 161-193
- Zapotocnt, T. H., Nieman, S. J., Menzel, W. P., Nelson III, J. P., Jung, J. A., Rogers, E., Parrish, D. F., DiMego, G. J., Baldwin, M. and Schmit, T. J. , 2000: Study of the sensitivity of the data assimilation system. *Wea. Forecasting*, **15**, 603-621.
- Zhang, J, F. Carr and K. Brewster, 1998: Impact of initial cloud analysis on storm-scale precipitation forecasts. *16<sup>th</sup> Conf. Wea. Analysis and Forecast.* Amer. Meteor. Soc., Phoenix, AZ.

**Figure captions:**

**Figure 1.** (a) 50 km coarse grid located in a Europe map, (b) 10 km ARPS grid located in coarse grid, and (c) ARPS topography on the 10 km grid. Contours and grey shading contrasts at 0, 100, 300, 500, 700, 900, 1200 and 1500 m. Monthly medium precipitation is given in Table 1 for stations A through E and comparison of forecast and observed daily total precipitation is given in Fig. 12 for stations marked as M, I and P.

**Figure 2.** Scheme of the daily operational forecast for Galician region

**Figure 3.** Relationship between cloud cover and relative humidity at different height levels (Reproduced from Zhang, 1999)

**Figure 4.** Entrainment reduction curve (Reproduced from Zhang, 1999)

**Figure 5.** Comparison of total precipitation over Galicia during November 2000 measured (numbers in boxes) and that predicted by ARPS using cloud water initialization (contours and grey shading contrasts at 100, 200, 300, 400, 500, 600 and 800 mm)

**Figure 6.** Synoptic analysis for 5 November 2000 at 0600 UTC, 1200 UTC and 1800 UTC. Adopted from INM (National Weather Service of Spain) bulletins. B symbol in the figure indicates the low pressure center, derived from Spanish word *baja*

**Figure 7.** Sea level pressure (contours) and 850hPa temperature (shaded field) predicted by ARPS on 50 km coarse grid for 5 November, 2000 at 0600 UTC, 1200 UTC and 1800 UTC.

**Figure 8.** Vertical integrated rain water mixing ratio ( $q_r$ ) predicted with ARPS on the fine grid at 1200 UTC on 5 November 2000 with (a) and without (b) cloud initialization. The model started from 00Z 5 November initial condition based on the 12 hour AVN forecast background.

**Figure 9.** Surface wind velocity predicted by ARPS on 10 km fine grid at 1500 UTC 5 November 2000.

**Figure 10.** Surface wind velocity and direction comparison between measurements at A (in the W coast, 5m) and B (in the SE mountains, 970 m) stations, and model results, on 5<sup>th</sup> November 2000.

**Figure 11.** Comparison between total rainfall over Galicia for 5 November 2000 predicted by ARPS with (a) and without (b) cloud initialization and observations (numbers in boxes)

**Figure 12.** Differences in equivalent potential temperature (0.2 K intervals) at 500 hPa between runs with and without cloud water initialization at 1500 UTC. Also shown are surface fronts based on synoptic data at same time

**Figure 13.** Comparison of daily total precipitation measured (bars) and predicted by ARPS (line) in MOUR station (8.14W, 42.61N), INVE station (7.34W, 42.12N) and PMUR station (7.08W, 43.54N). These stations are marked at M, I and P in Fig. 1c

**Figure 14.** 1 hour accumulated precipitation measured (black bars) and predicted (dots) at MOUR location for 5th November 2001

**Figure 15.** Scatterplots of ARPS and observed precipitation (mm) with (a) and without (b) cloud initialization for 5th November 2000. For reference, the 1-to-1 and 2-to-1 lines are solid and dotted, respectively.

**Figure 16.** Monthly mean value of bias and threat score for various precipitation thresholds (mm/24h) for November, 2000

***Table captions:***

**Table 1.** Monthly mean value of days with precipitation of 1 mm or more and the annual mean value (last column) measured at five different sites (A, B, C, D, E, indicated in Fig. 1c)

**Table 2.** Skill scores for ARPS model at the meteorological stations. Labels on heading denote thresholds used to evaluate each score, in mm of precipitation. Only days with observed precipitation are shown.

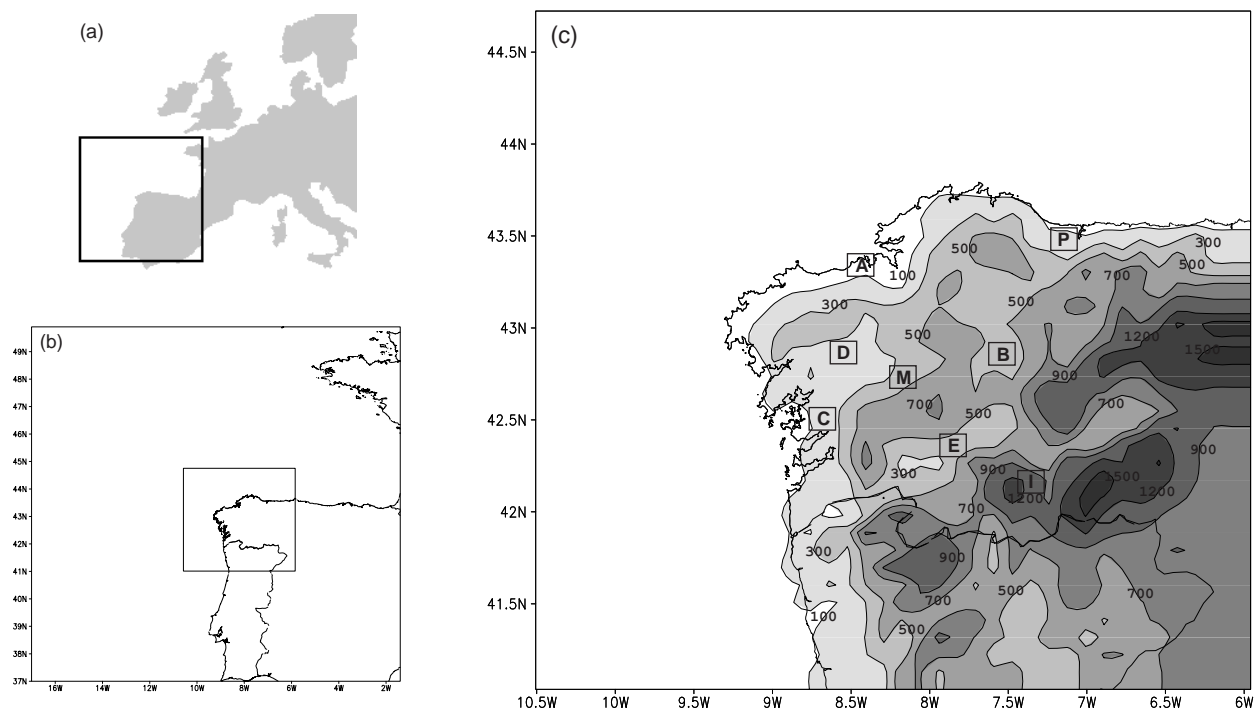


**Figure 1.** (a) 50 km coarse grid located in a Europe map, (b) 10 km ARPS grid located in coarse grid, and (c) ARPS topography on the 10 km grid. Contours and grey shading contrasts at 0, 100, 300, 500, 700, 900, 1200 and 1500 m. Monthly medium precipitation is given in Table 1 for stations A through E and comparison of forecast and observed daily total precipitation is given in Fig. 12 for stations marked as M, I and P.

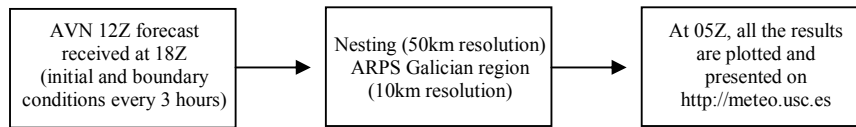


**Figure 2.** Schematic of the daily operational forecast for the Galician region

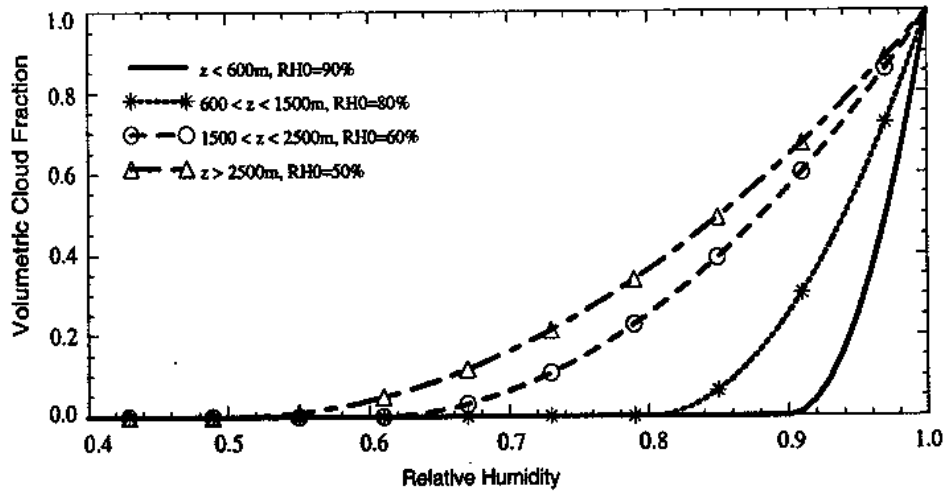


**Figure 3.** Relationship between cloud cover and relative humidity at different height levels (Reproduced from Zhang, 1999)

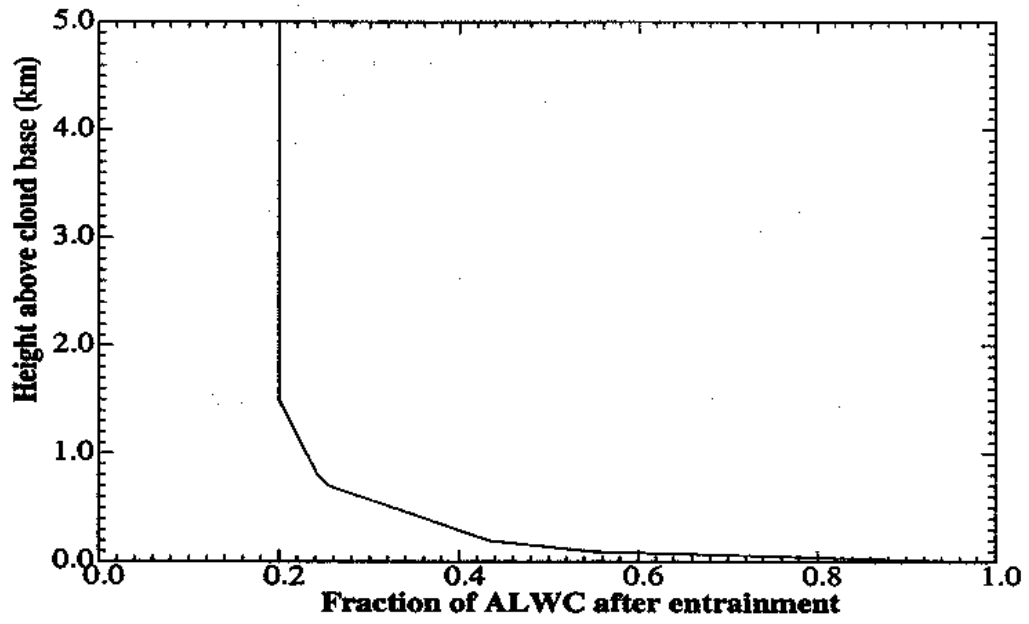
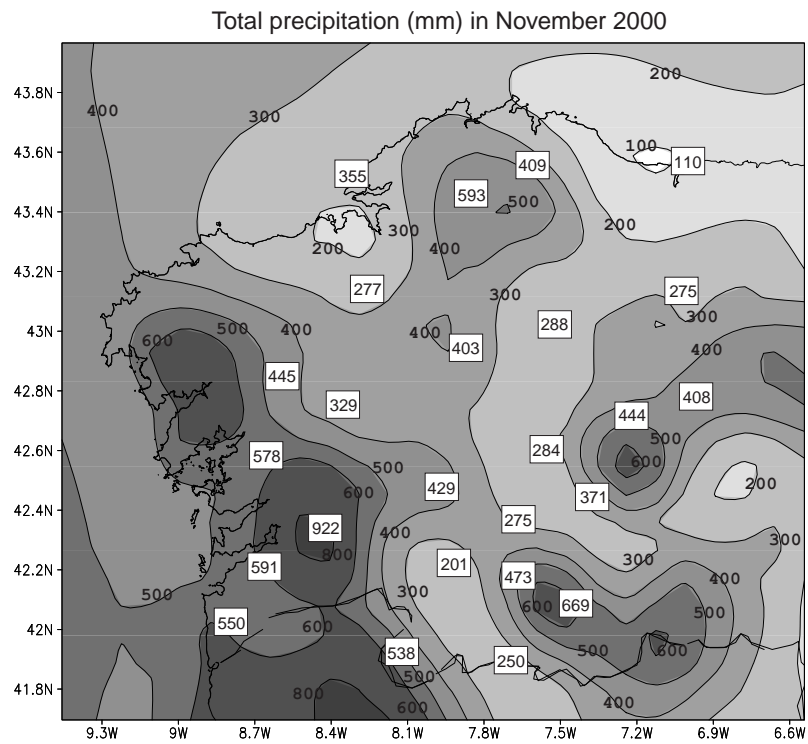
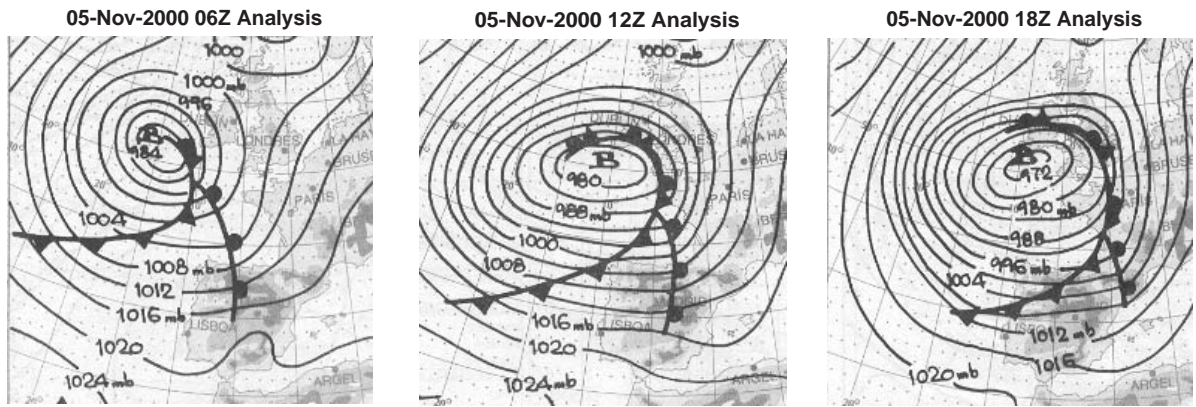


Figure 4. Entrainment reduction curve (Reproduced from Zhang, 1999)



**Figure 5.** Comparison of total precipitation over Galicia during November 2000 measured (numbers in boxes) and that predicted by ARPS using cloud water initialization (contours and grey shading contrasts at 100, 200, 300, 400, 500, 600 and 800 mm)



**Figure 6.** Synoptic analysis for 5 November, 2000 at 0600 UTC, 1200 UTC and 1800 UTC. Adopted from INM (National Weather Service of Spain) bulletins. B symbol in the figure indicates the low pressure center, derived from Spanish word *baja*.

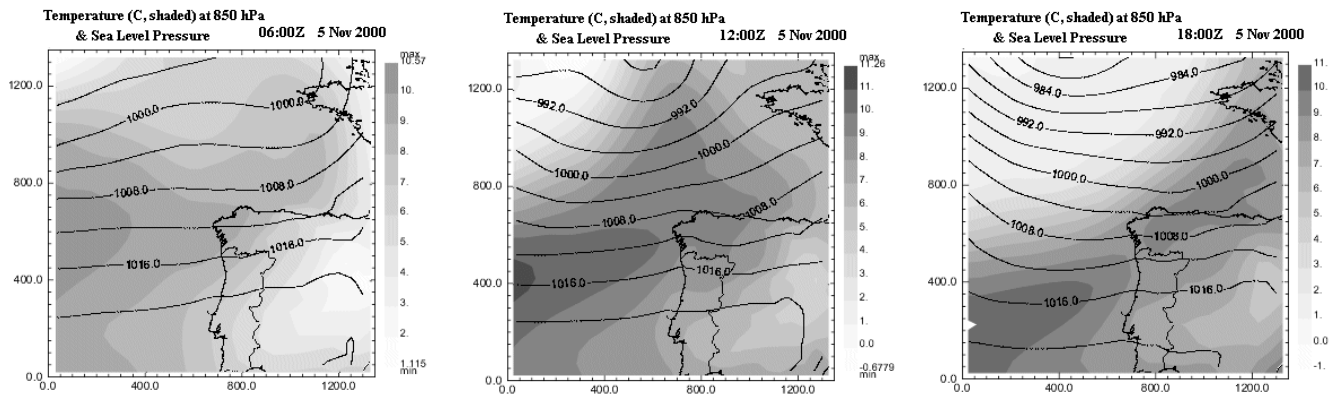


**Figure 7.** Sea level pressure (contours) and 850hPa temperature (shaded field) predicted by ARPS on 50 km coarse grid for 5 November, 2000 at 0600 UTC, 1200 UTC and 1800 UTC.

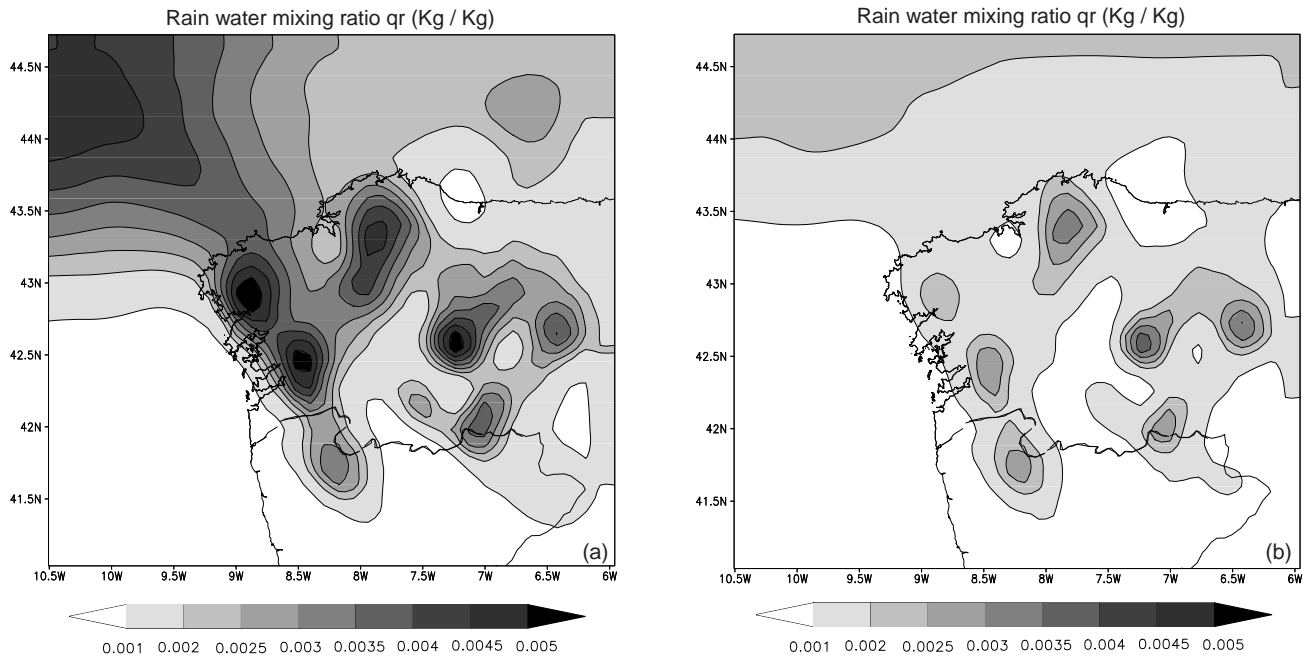


**Figure 8.** Vertical integrated rain water mixing ratio ( $q_r$ ) predicted with ARPS on the fine grid at 1200 UTC on 5 November 2000 with (a) and without (b) cloud initialization. The model started from 00Z 5 November initial condition based on the 12 hour AVN forecast background.

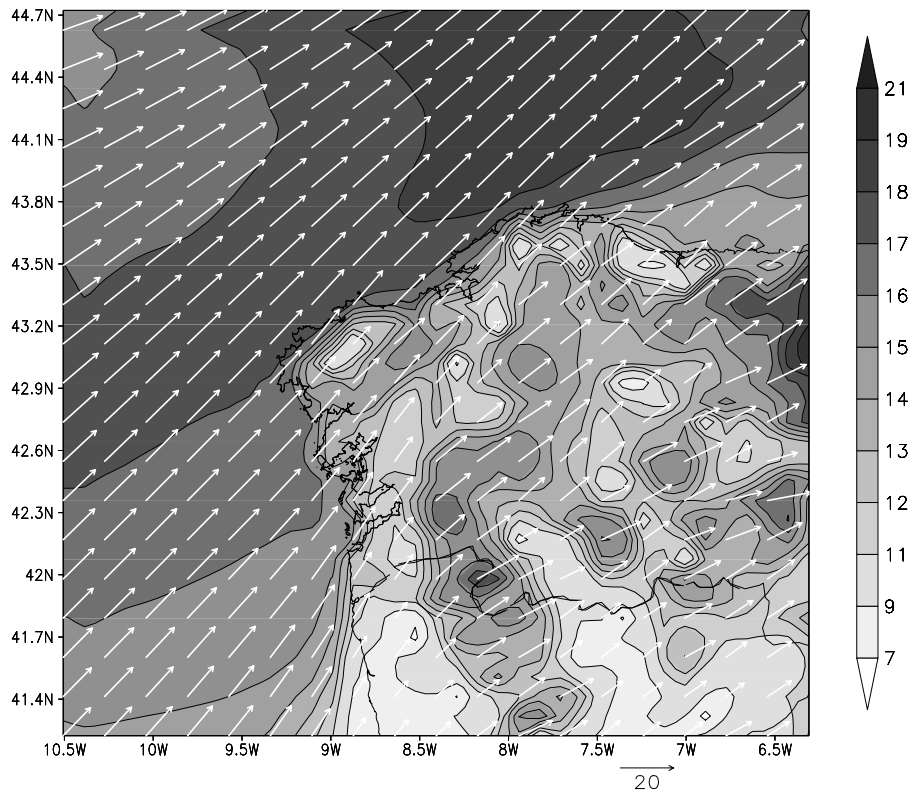


**Figure 9.** Surface wind velocity (shaded) and wind direction (vectors) predicted by ARPS on 10 km fine grid at 1500 UTC, 5 November 2000

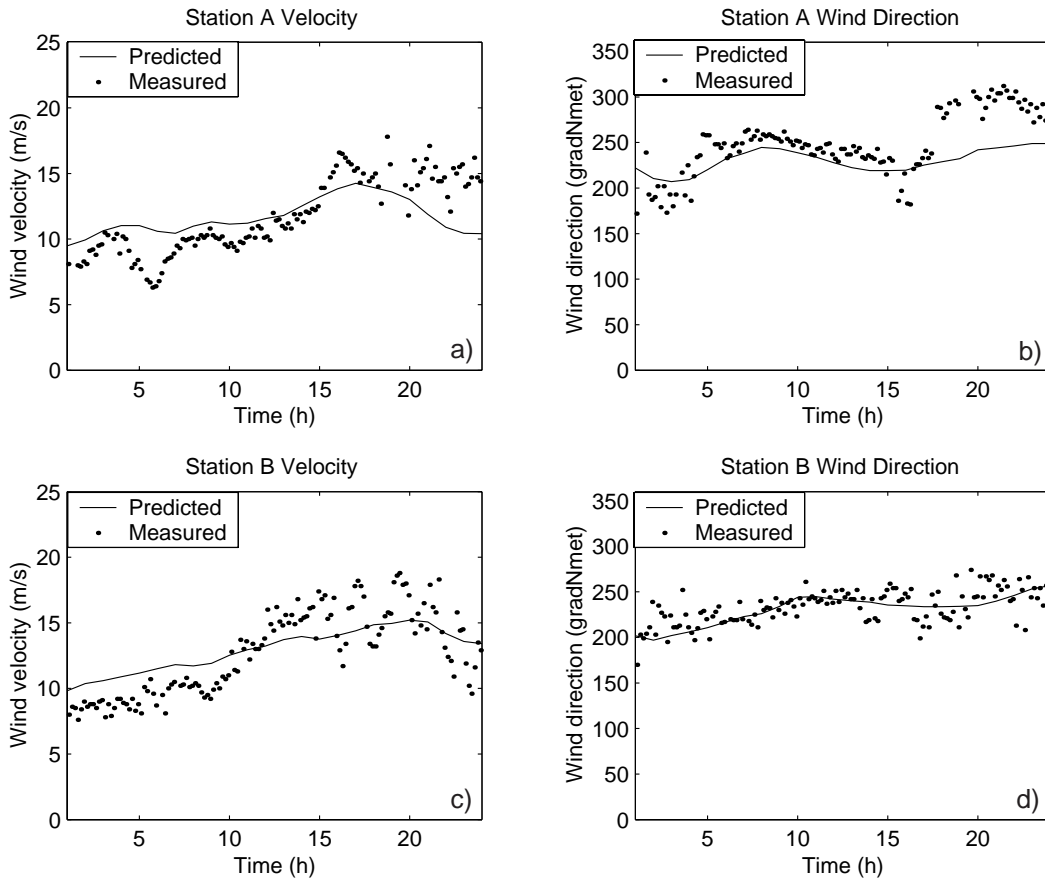


**Figure 10.** Surface wind velocity and direction comparison between measurements at A (in the W coast, 5m) and B (in the SE mountains, 970 m) stations, and model forecast, on 5th November 2000.

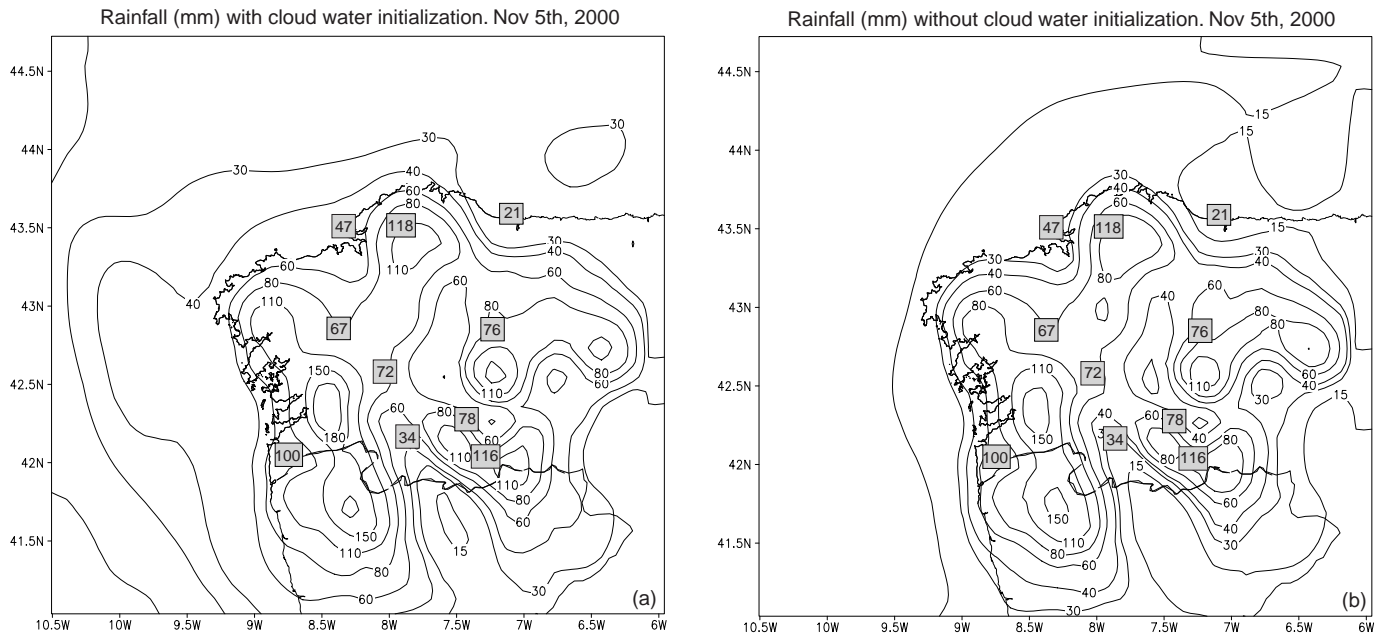


**Figure 11.** Comparison between total rainfall over Galicia for 5, November, 2000 predicted by ARPS with (a) and without (b) cloud initialization and observations (numbers in boxes)

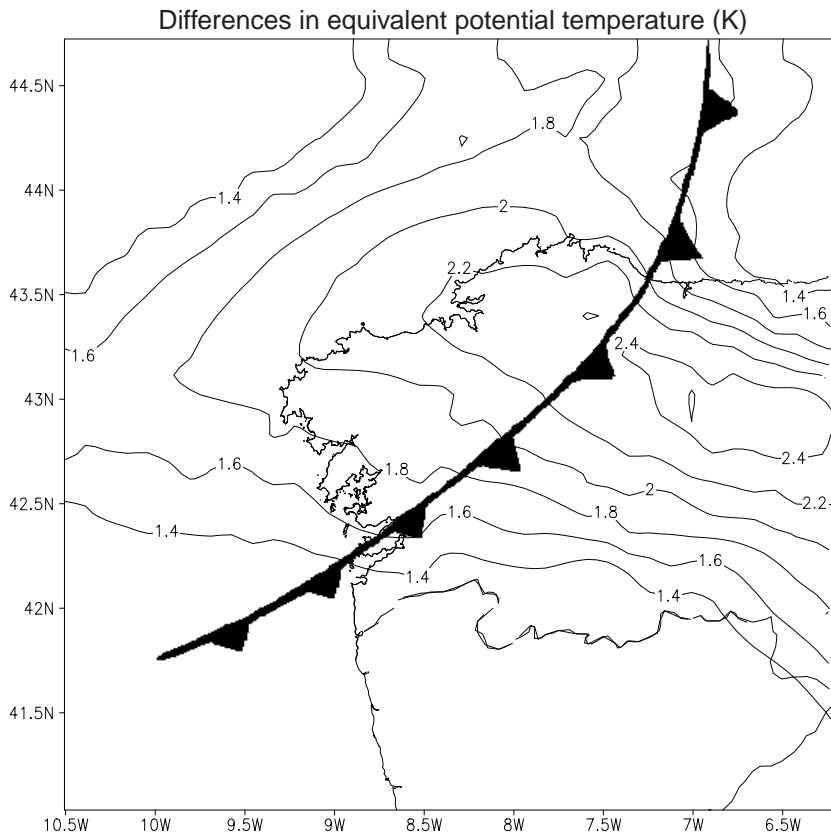


**Figure 12.** Differences in equivalent potential temperature (0.2 K intervals) at 500 hPa between runs with and without cloud water initialization at 1500 UTC. Also shown are surface fronts based on synoptic data at same time.

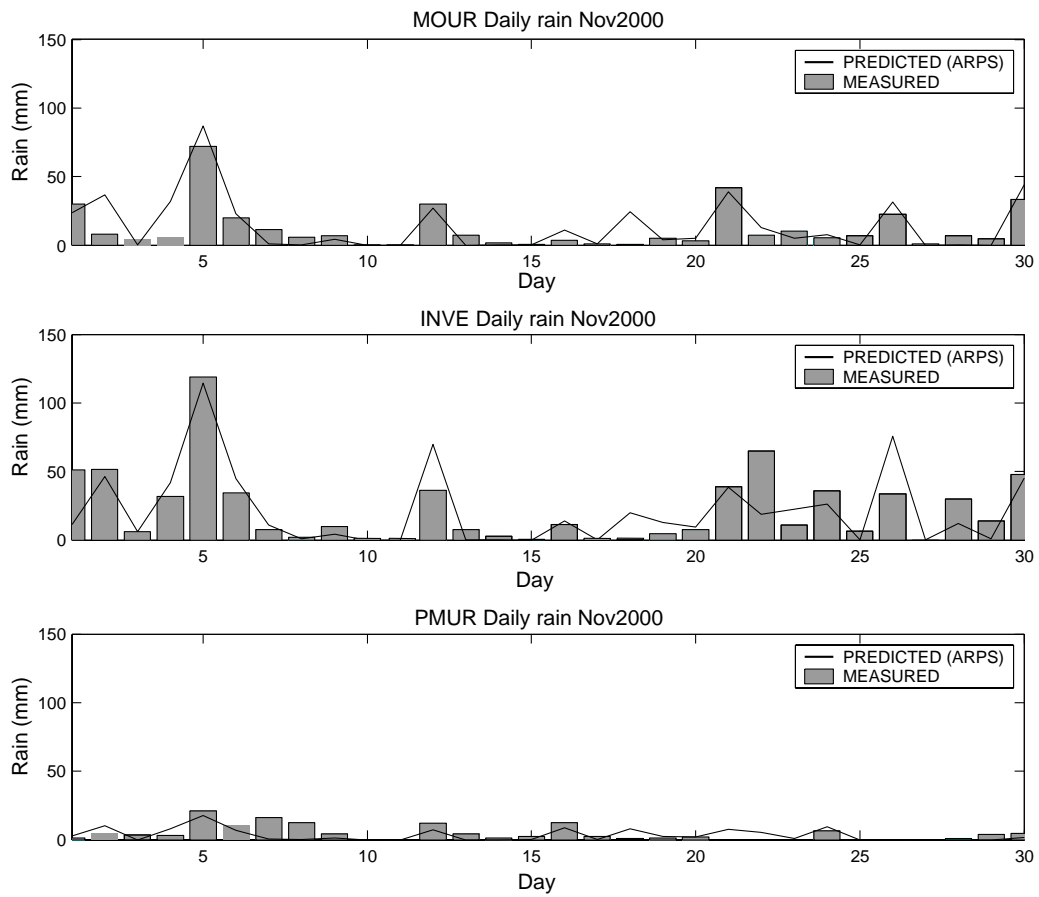


**Figure 13.** Comparison of daily total precipitation measured (bars) and predicted by ARPS (line) in MOUR station (8.14W, 42.61N), INVE station (7.34W, 42.12N) and PMUR station (7.08W, 43.54N). These stations are marked at M, I and P in Fig. 1c

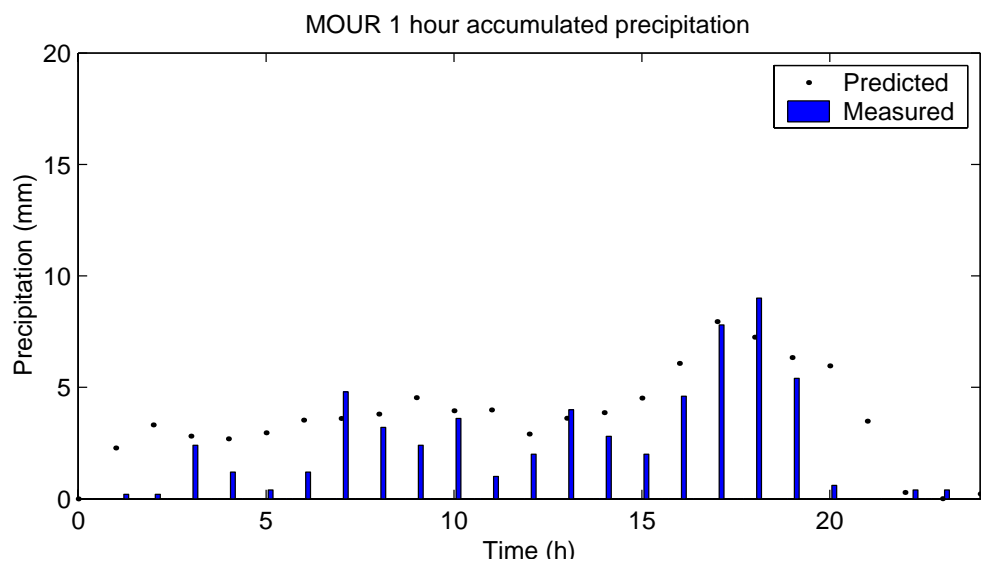


**Figure 14.** 1 hour accumulated precipitation measured (black bars) and predicted (dots) at MOUR location for 5<sup>th</sup> November 2001

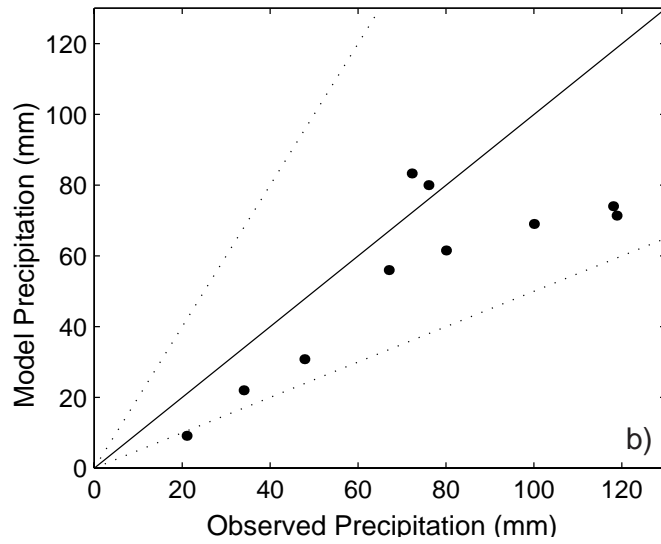
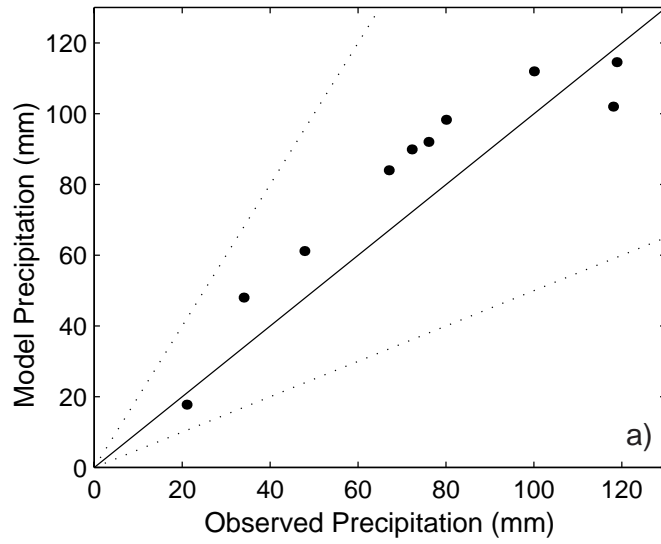


**Figure 15.** Scatter diagrams of observed precipitation (mm) and model forecasts with (a) and without (b) cloud initialization, for 5 November 2000. For reference, the 1-to-1 and 2-to-1 lines are solid and dotted, respectively.

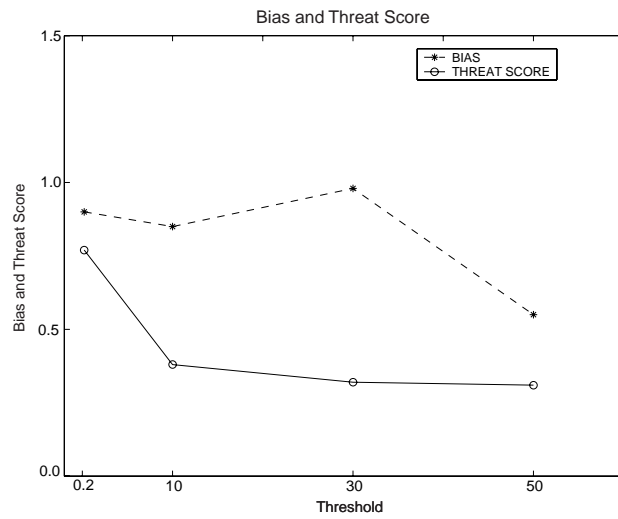


**Figure 16.** Monthly mean value of bias and threat score for various precipitation thresholds (mm/24h) for November, 2000.

	JAN	FEB	MAR	APR	MAY	JUN	JUL	AUG	SEP	OCT	NOV	DEC	ANNUAL
A	17.3	16.7	16.5	16.6	15.3	9.8	7.1	8.7	10.2	15.0	17.2	17.4	167.8
B	18.9	18.0	18.0	16.4	16.5	10.1	8.6	9.8	13.0	15.9	18.4	19.1	182.7
C	16.3	16.3	15.1	13.1	14.5	8.5	6.0	6.0	9.6	12.8	14.3	15.9	148.4
D	18.2	17.3	16.6	15.8	15.6	9.6	6.4	7.4	10.1	14.7	16.6	16.7	165.0
E	14.2	13.9	12.7	13.1	12.2	6.8	4.2	4.3	6.2	11.9	12.1	14.4	126.0

**Table 1.** Monthly mean value of days with precipitation of 1mm or more and the annual mean value (last column) measured at five different sites (A, B, C, D, E, indicated in Fig. 1c)

<i>Date</i>	<b>Bias</b>				<b>Threat Score</b>			
	<i>0.2</i>	<i>10.</i>	<i>30.</i>	<i>50.</i>	<i>0.2</i>	<i>10.</i>	<i>30.</i>	<i>50.</i>
01 Nov	1.0	1.17	0.67	0.0	1.0	0.63	0.25	0.0
02 Nov	1.0	2.25	2.0	1.0	1.0	0.44	0.5	1.0
03 Nov	0.33	0.0	-	-	0.33	0.0	-	-
04 Nov	1.0	1.6	3.0	-	1.0	0.63	0.33	-
05 Nov	1.0	1.0	1.4	1.75	1.0	1.0	0.71	0.57
06 Nov	1.0	1.0	2.0	-	1.0	1.0	0.5	-
07 Nov	0.78	0.14	-	-	0.78	0.0	-	-
08 Nov	0.63	0.0	0.0	-	0.63	0.0	0.0	-
09 Nov	1.0	0.0	-	-	1.0	0.0	-	-
10 Nov	0.0	-	-	-	0.0	-	-	-
12 Nov	1.0	0.89	0.6	-	1.0	0.89	0.33	-
13 Nov	0.0	0.0	-	-	0.0	0.0	-	-
14 Nov	0.75	-	-	-	0.56	-	-	-
15 Nov	2.0	-	-	-	0.5	-	-	-
16 Nov	1.0	3.5	-	-	1.0	0.13	-	-
17 Nov	1.6	-	-	-	0.63	-	-	-
18 Nov	1.6	0.0	-	-	0.63	0.0	-	-
19 Nov	1.0	0.25	-	-	1.0	0.0	-	-
20 Nov	1.0	0.5	-	-	1.0	0.0	-	-
21 Nov	1.0	1.0	0.83	-	1.0	1.0	0.83	-
22 Nov	1.0	2.0	0.0	0.0	1.0	0.29	0.0	0.0
23 Nov	1.0	2.0	-	-	1.0	0.5	-	-
24 Nov	1.0	1.25	0.0	-	1.0	0.8	0.0	-
25 Nov	0.6	0.0	-	-	0.6	0.0	-	-
26 Nov	1.0	1.0	2.0	-	1.0	1.0	0.5	-
28 Nov	0.67	0.0	0.0	-	0.67	0.0	0.0	-
29 Nov	0.29	0.0	-	-	0.29	0.0	-	-
30 Nov	1.0	0.83	0.25	0.0	1.0	0.83	0.25	0.0

**Table 2.** Skill scores for ARPS model at the meteorological stations. Labels on heading denote thresholds used to evaluate each score, in mm of precipitation. Only days with observed precipitation are shown.